NMR and INS Line Shapes of Transition Metal Hydrides in the Presence of Coherent and Incoherent Dihydrogen Exchange

Hans-Heinrich Limbach,*,† Stefan Ulrich,† Stephan Gründemann,† Gerd Buntkowsky,† Sylviane Sabo-Etienne,‡ Bruno Chaudret,‡ Gregory J. Kubas,§ and Jürgen Eckert§

Contribution from the Institut für Organische Chemie der Freien Universität Berlin, Takustrasse 3, D-14195 Berlin, Germany, the Laboratoire de Chimie de Coordination du CNRS (UP 8241), 205, route de Narbonne, F-31077 Toulouse-Cedex, France, and LANSCE, Los Alamos National Laboratory, Los Alamos, Mail Stop H805, New Mexico 87545

Received August 19, 1996. Revised Manuscript Received May 19, 1998

Abstract: In this paper a unified description of the effects of the coherent and incoherent dihydrogen exchange on the NMR and INS spectra of transition metal hydrides based on the quantum-mechanical density matrix formalism of Alexander−Binsch is proposed. The dynamic parameters of the line shape analyses are the exchange couplings or rotational tunnel splittings J of the coherent exchange and the rate constants k of the incoherent exchange. As experimental examples, we report the temperature dependent values J and k for **1** ≡ $Cp^*RuH_3(PCy_3)$ ($Cp^* \equiv C_5(CH_3)_5$ and Cy ≡ cyclohexyl) including the kinetic HH/HD/DD isotope effects on the incoherent exchange, determined by NMR, and for the tungsten dihydrogen complex **2** ≡ $W(PCy_3)_2(CO)_3(\eta\text{-}H_2)$, determined by INS. The temperature dependence of J and k is interpreted qualitatively in terms of a simple reaction scheme involving at each temperature a ground state and a dominant ro-vibrationally excited state. Using formal kinetics it is shown that a coherent exchange in the excited state contributes to J only if this exchange presents the rate limiting reaction step, i.e., if vibrational deactivation is fast. This is the case for levels located substantially below the top of the barrier. A very fast coherent exchange of levels located close to the top of the barrier contributes only to k. This result reproduces in a simple way the quantum-mechanical results of Szymanski, S. *J. Chem. Phys.* **1996**, *104*, 8216 and Scheurer, C.; Wiedenbruch, R.; Meyer, R.; Ernst, R. R. *J. Chem. Phys.* **1997**, *106*, 1. The results concerning the coherent and incoherent exchange processes in **1** and **2** are discussed in terms of the simplified reaction model.

Introduction

Transition metal hydrides exhibit interesting exchange phenomena of metal bound dihydrogen pairs.[1−14] As depicted in Figure 1a, the exchange can be either "coherent", corresponding in the time domain to a periodic quantum exchange or a rotational tunnel process or it can be "incoherent", corresponding to a stochastic rate process. The former can be characterized by the tunnel frequency or exchange coupling J and the latter by the rate constant k. By contrast, the related exchange of chlorins and porphyrins (Figure 1b) is always incoherent.[15] The topic of this paper is, therefore, the relation between the coherent and the incoherent exchange in transition metal complexes whose knowledge might eventually lead to an understanding why the two classes of compounds behave in a different way.

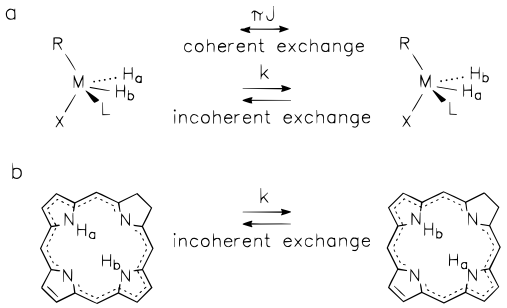

Figure 1. (a) Coherent vs incoherent dihydrogen exchange in transition metal hydrides. (b) Incoherent exchange in chlorin.[15]

For this purpose, let us first review some experimental findings concerning both kinds of exchange processes. As shown in the case of η-bound dihydrogen complexes,[2,3] the coherent exchange leads to characteristic transitions in the low-temperature Inelastic Neutron Scattering (INS) spectra if J is of the order of GHz to THz. On the other hand, in the case of typical di- or trihydride complexes J is of the order of Hz to kHz and giving rise to "exchange couplings" between the NMR signals of the exchanging hydrogen nuclei,[5,6] as shown by Zilm[6a−d] and Weitekamp.[6e] In the NMR case, J is found to strongly increase with increasing temperature indicating a dynamic average over many ro-vibrational states, configurations,

† Institut für Organische Chemie der Freien Universität Berlin.
‡ Laboratoire de Chimie de Coordination du CNRS.
§ LANSCE, Los Alamos National Laboratory.

(1) Presented partly at the *1st and 2nd Symposia on Hydrogen and Quantum Mechanical Phenomena in the Coordination Sphere of Transition Metals*; Toulouse, February, 17−19, 1994 and Santa Fe, NM, December 13−15, 1995.

(2) (a) Kubas, G. J.; Ryan, R. R.; Swanson, B. I.; Vergamini, P. J.; Wasserman, H. J. *J. Am. Chem. Soc.* **1984**, *106*, 451. (b) Kubas, G. J. *Acc. Chem. Res.* **1988**, *21*, 120.

(3) (a) Rattan, G.; Kubas, G. J.; Unkefer, C. J.; Van Der Sluys, L. S.; Kubat-Martin, K. A.; *J. Am. Chem. Soc.* **1990**, *112*, 3855. (b) Van Der Sluys, L. S.; Eckert, J.; Eisenstein, O., Hall, J. H.; Huffman, J. C.; Jackson, S. A.; Koetzle, T. F.; Kubas, G. J.; Vergamini, P. J.; Caulton, K. G. *J. Am. Chem. Soc.* **1990**, *112*, 4831. (c) Eckert, J.; Kubas, G. J. *J. Phys. Chem.* **1993**, *97*, 2378. (d) Eckert, J.; Kubas, G. J.; White, R. P. *Inorg. Chem.* **1993**, *31*, 1550. (e) Eckert, J.; Kubas, G. J.; Dianoux, A. J. *J. Chem. Phys.* **1988**, *88*, 466. (f) Eckert, J.; Jensen, C. M.; Jones, G.; Clot, E.; Eisenstein, O. *J. Am. Chem. Soc.* **1993**, *115*, 11056.

(4) Jessop, P. G.; Morris, R. J. *Coord. Chem. Rev.* **1992,** *121*, 155.

S0002-7863(96)02903-4 CCC: $15.00
Published on Web 07/28/1998

and solvent environments exhibiting different intrinsic J values. Various models explaining the temperature dependence of J have been proposed, based either on exchange in a one- or two-dimensional double well potential[6,14] or on rotational tunneling in dihydrogen-like configurations.[1,7,8b] On the other hand, the incoherent exchange leads to a broadening and coalescence of the NMR signals of the hydrogen nuclei in different chemical sites. The NMR phenomena have experimentally been observed and reproduced[5h,i,m−p,8] in terms of a superimposed coherent and incoherent exchange using the well-known quantum-mechanical density matrix formalism of Alexander and Binsch.[16] A theoretical foundation of this use of the Alexander−Binsch formalism in this context was provided by Szymanski.[11] This formalism is also able to describe para-H_2 induced NMR phenomena in hydrogenation reactions.[17] In the case of the INS spectra, only line broadening is observed when the temperature is increased.

As we did not see a principal difference between the dihydrogen dynamics observed by NMR and INS we suspected that the INS line broadening could also be described in a similar way as the NMR observations. Therefore, we study in the theoretical section the effects of a superimposed coherent and incoherent exchange on both the INS and NMR line shapes using the Alexander−Binsch formalism. The advantage of this description is that it allows one to directly compare the dynamic parameters J and k of exchange obtained both by NMR and by INS. Thus, it is no longer necessary to formulate separate rigorous quantum-mechanical INS[18,19] and NMR[11,12] theories but only a single theory of J and k. As experimental NMR example, we report in this paper new NMR results obtained for $Cp^*RuH_3(PCy_3)$ ($Cp^* \equiv C_5(CH_3)_5$ and Cy ≡ cyclohexyl, **1**) and its deuterated isotopologs dissolved in organic liquids down to 160 K. **1** was one of the first compounds reported to exhibit quantum exchange couplings at low and a classical exchange at higher temperatures.[5a−c] As an INS example, we reanalyze the temperature-dependent INS spectra[3e] of the Kubas dihydrogen complex $W(PCy_3)_2(CO)_3(\eta\text{-}H_2)$ **2** in terms of the Alexander−Binsch theory.

In order to understand in more detail the relation between the coherent and incoherent exchange we treat in the theoretical section a simple four-state reaction model depicted in Figure 2 which provides a qualitative explanation of the temperature dependence of both the coherent exchange which dominates at low and the incoherent exchange which dominates at high temperatures. The model involves two quasi-degenerate ground states A and A′ which do not exchange directly but via excited states B and B′ which contribute—depending on their energy and exchange dynamics—either to the overall values of J or of k. At low temperatures excited states with well defined HH-vector orientations will dominate, located well below the top of the barrier (Figure 2a). By contrast, at high temperatures levels located close to the top of the barrier exhibiting delocalized hydrogen vector orientations (Figure 2c) will dominate the overall exchange. In the case of Figure 2b the HH vectors exhibit a 90° rotation during the formation of the excited state B and B′. The latter may correspond to dihydrogen-like configurations as proposed previously,[7a] but they do not necessarily need to represent stationary states because vibrational relaxation can be treated in a similar way as chemical kinetics. It will be shown using formal kinetic methods that the overall exchange between A and A′ is incoherent with exception of the case of Figure 2a, and only when the rate limiting step of the reaction scheme corresponds to a coherent exchange between B and B′. Similar results have been derived

(5) (a) Arliguie, T.; Chaudret, B.; Devillers, J.; Poilblanc, R. *C. R. Acad. Sci. Paris, Ser. II* **1987,** *305*, 1523. (b) Antiñolo, A.; Chaudret, B.; Commenges, G.; Fajardo, M.; Jalon, F.; Morris, R. H.; Otero, A.; Schweitzer, C. T.; *J. Chem. Soc., Chem. Commun.* **1988**, 1210. (c) Arliguie, T.; Border, C.; Chaudret, B.; Devilles, J.; Poilblanc, R. *Organometallics* **1989**, *8*, 1308. (d) Arliguie, T.; Chaudret, B.; Jalon, F. A.; Otero, A.; Lopez, J. A.; Lahoz, F. J. *Organometallics* **1991**, *10*, 1888. (e) Paciello, R. R.; Manriquez, J. M.; Bercaw, J. E. *Organometallics* **1990**, *9*, 260. (f) Heinekey, D. M.; Payne, N. G.; Schulte, G. K. *J. Am. Chem. Soc.* **1988**, *110*, 2303. (g) Heinekey, D. M.; Millar, J. M.; Koetzle, T. F.; Payne, N. G.; Zilm, K. W. *J. Am. Chem. Soc.* **1990**, *112*, 909. (h) Limbach, H. H.; Scherer, G.; Meschede, L.; Aguilar-Parrilla, F.; Wehrle, B.; Braun, J.; Hoelger, Ch.; Benedict, H.; Buntkowsky, G.; Fehlhammer, W. P.; Elguero, J.; Smith, J. A. S.; Chaudret, B. *NMR Studies of Elementary Steps of Hydrogen Transfer in Condensed Phases*. In *Ultrafast Reaction Dynamics and Solvent Effects, Experimental and Theoretical Aspects*; Gauduel, Y., Rossky, P. J., Eds.; American Institute of Physics: 1994; Chapter 2, p 225. (i) Antiñolo, A.; Carrillo, F.; Chaudret, B.; Fajardo, M.; Fernandez-Baeza, J.; Lanfranchi, M.; Limbach, H. H.; Maurer, M.; Otero, A.; Pellinghelli M. A. *Inorg. Chem.*, **1994**, *33*, 5163. (k) Chaudret, B., Limbach, H. H., Moise, C. *C. R. Acad. Sci. Paris, Ser. II* **1992**, *315*, 533. (l) Ayllon, J. A., Sabo-Etienne, S.; Chaudret, B.; Ulrich, S.; Limbach, H. H. *Inorg. Chim. Acta* **1997**, *259*, 1. (m) Wiedenbruch, R.; Schick, M.; Pampel, A.; Meier, B. H.; Meyer, R.; Ernst, R. R.; Chaloupka, A.; Venanzi, L. M. *J. Phys. Chem.* **1995**, *99*, 13088. (n) Heinekey, D. M.; Hinkle, A. S.; Close, J. D. *J. Am. Chem. Soc.* **1996**, *118*, 5353. (o) Heinekey, D. M.; Payne, N. G.; Sofield, C. D. *Organometallics* **1990**, *9*, 2643. (p) Heinekey, D. M.; van Roon, M. *J. Am. Chem. Soc.* **1996**, *118*, 12134.

(6) (a) Zilm, K. W.; Heinekey, D. M.; Millar, J. M.; Payne, N. G.; Demou, P. *J. Am. Chem. Soc.* **1989**, *111*, 3088. (b) Zilm, K. W.; Heinekey, D. M.; Millar, J. M.; Payne, N. G.; Neshyba, S. P.; Duchamp, J. C.; Szczyrba, J. *J. Am. Chem. Soc.* **1990**, *112*, 920. (c) Zilm, K. W.; Millar, J. M. A*dv. Magn. Reson.* **1990**, *15*, 16. (d) Inati, S. J.; Zilm, K. W.; *Phys. Rev. Lett.* **1992**, *68*, 3273. (e) Jones, D.; Labinger, J. A.; Weitekamp, J. *J. Am. Chem. Soc.* **1989**, *111*, 3087. (f) Szymanski, S. *J. Mol. Struct.* **1994**, *321*, 115.

(7) (a) Limbach, H. H.; Scherer, G.; Maurer, M.; Chaudret, B. *Angew. Chem.* **1992**, *104*, 1414; *Angew. Chem., Int. Ed. Engl.* **1990**, *31*, 1369. (b) Gründemann, S.; Limbach, H. H.; Rodriguez, V.; Donnadieu, B.; Sabo-Etienne, S.; Chaudret, B. *Ber. Bunsenges. Phys. Chem.* **1998**, *102*, 344.

(8) (a) Barthelat, J. C.; Chaudret, B.; Daudey, J. P.; De Loth, Ph.; Poilblanc, R. *J. Am. Chem. Soc.* **1991**, *113*, 9896. (b) Sabo-Etienne, S.; Chaudret, B.; El-Makarim, H. A.; Barthelat, J. C.; Daudey, J. P.; Ulrich, S.; Limbach, H. H.; Moíse, C. *J. Am. Chem. Soc.* **1995**, *117*, 11602.

(9) (a) Clot, E. Ph.D. Thesis, June 1995 Université de Paris-Sud, France. (b) Clot, E.; Leforestier, C.; Eisenstein, O.; Pelissier, M. *J. Am. Chem. Soc.* **1995**, *117*, 1797. (c) Kuhlmann, R.; Clot, E.; Leforestier, C.; Streib, W. E.; Eisenstein, O.; Kaulton, K. G.; *J. Am. Chem. Soc.* **1997**, *119*, 10153. (d) Jarid, A.; Moreno, M.; Lled¢s, A.; Lluch, J. M.; Bertran, J. *J. Am. Chem. Soc.* **1993**, *115*, 5861. (e) Jarid, A.; Moreno, M.; Lledos, A.; Lluch, J. M.; Bertran, J. *J. Am. Chem. Soc.* **1995**, *117*, 1069.

(10) (a) Hiller, E. M.; Harris, R. A. *J. Chem. Phys.* **1993**, *98*, 2077. (b) Hiller, E. M.; Harris, R. A. *J. Chem. Phys.* **1993**, *99*, 7652. (c) Hiller, E. M.; Harris, R. A. *J. Chem. Phys.* **1993**, *100*, 2522.

(11) Szymanski, S. *J. Chem. Phys.* **1996**, *104*, 8216.

(12) Scheurer, C.; Wiedenbruch, R.; Meyer, R.; Ernst, R. R. *J. Chem. Phys.* **1997**, *106*, 1.

(13) (a) Landesmann, A. *Ann. Phys. (Fr.)* **1973**, *8*, 53. (b) Close, J. D. *J. Chem. Phys.* **1996**, *105*, 2317.

(14) Buntkowsky, G.; Limbach, H. H.; Wehrmann, F.; Sack, I.; Vieth, H. M.; Morris, R. H. *J. Phys. Chem. A* **1997**, *101*, 4679.

(15) (a) Schlabach, M.; Wehrle, B.; Limbach, H. H.; Bunnenberg, E.; Knierzinger, A.; Shu, A.; Tolf, B. R.; Djerassi, C. *J. Am. Chem. Soc.* **1986**, *108*, 3856. (b) Schlabach, M.; Rumpel, H.; Limbach, H. H., *Angew. Chem.* **1989**, *101*, 84; *Angew. Chem., Int. Ed. Engl.* **1989**, *28*, 76. (c) Schlabach, M.; Scherer, G.; Limbach, H. H. *J. Am. Chem. Soc.* **1991**, *113*, 3550. (d) Braun, J.; Schlabach, M.; Wehrle, B.; Köcher, M.; Vogel, E.; Limbach, H. H. *J. Am. Chem. Soc.* **1994**, *116*, 6593. (e) Braun, J.; Limbach, H. H.; Williams, P. G.; Morimoto, H.; Wemmer, D. E. *J. Am. Chem. Soc.* **1996**, *118*, 7231. (f) Braun, J.; Schwesinger, R.; Williams, P. G.; Morimoto, H.; Wemmer, D. E.; Limbach, H. H. *J. Am. Chem. Soc.* **1996**, *118*, 11101. (f) Brackhagen, O.; Scheurer, Ch.; Meyer, R.; Limbach, H. H. *Ber. Bunsenges. Phys. Chem.* **1998**, *102*, 303.

(16) (a) Alexander, S. *J. Chem. Phys.* **1962**, *37*, 971. (b) Binsch, G. J. *Am. Chem. Soc.* **1969**, *91*, 1304. (c) Kleier, D. A.; Binsch, G. *J. Magn. Reson.* **1970**, *3*, 146.

(17) Buntkowsky, G.; Bargon, J.; Limbach, H. H., *J. Am. Chem. Soc.* **1996**, 30, 8677.

(18) (a) Smith, D. *Chem. Rev.* **1994**, *94*, 1567. (b) Clough, S. *Physica* **1994**, *B202*, 256 and references cited therein. (c) Jahnke, T. K.; Müller-Warmuth, W.; Bennati, M. *Solid State NMR* **1995**, *4*, 153. (c) Heuer, A. *Z. Phys.* **1992**, *B88*, 39. (d) Press, W. *Single Particle Rotations in Molecular Crystals*; Springer: Berlin-Heidelberg-New York, 1981.

(19) (a) Hüller, A. *Z. Phys.* **1980**, *B36*, 215. (b) Würger, A. *Z. Phys.* **1989**, *B76*, 65. (c) Prager, M.; Heidemann, A. *Chem. Rev.* **1998**, *97*, 2933.

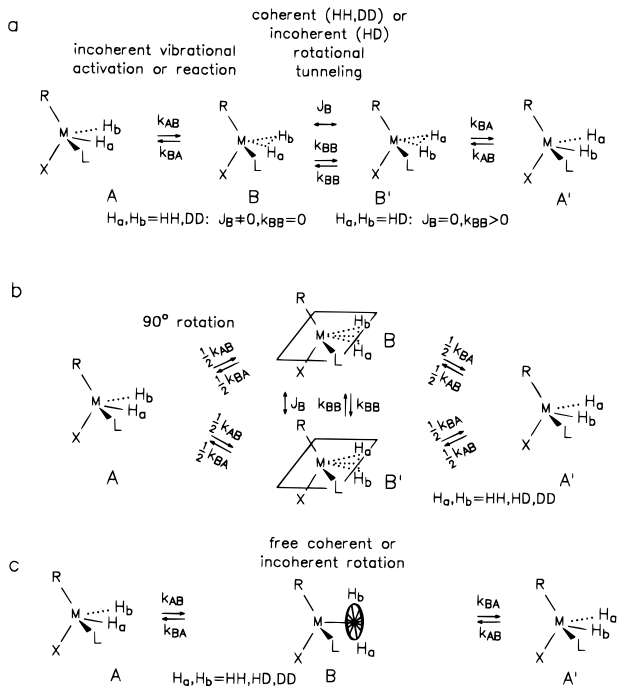

Figure 2. Dihydrogen exchange in transition metal hydrides between two near-degenerate ground states A and A′ via excited states B and B′. (a) B and B′ are located below the top of the barrier of exchange. The exchange between B and B′ is a coherent tunnel process in the case of a HH and a DD pair, characterized by the tunnel frequency J_B, and an incoherent process for a HD pair, characterized by the rate constant of incoherent tunneling k_{BB}. The overall exchange between A and A′ is only coherent if the exchange between B and B′ constitutes the rate limiting step. (b) B and B′ are located below the top of the barrier, but the activation is combined with a 90° rotation. The exchange between B and B′ does no longer influence the interconversion between A and A′. This mechanism is possible for all isotopic hydrogen pairs. (c) The intermediate state B is located above the barrier to rotation. The rate limiting step is the process of the formation of B. This mechanism is possible for all isotopic hydrogen pairs and represents the high temperature reaction channel corresponding to the mechanisms of (a) and (b).

by Szymanski[11] and Scheurer et al.[12] on a quantum-mechanical basis and resolve the problem of the calculated numerical instability of the average J at high temperatures.[9] The different exchange mechanisms of Figure 2 will imply different kinetic HH/HD/DD isotope effects on the incoherent exchange, a problem which will be qualitatively discussed in connection with the results obtained experimentally for **1**.

Theoretical Section

We use in the first part of this section the language of formal kinetics in order to describe the four-state models of Figure 2. In the second part of this section we present the description of both the NMR and the INS exchange broadened spectra in terms of the Alexander−Binsch formalism.

A Two-State Kinetic Treatment of Coherent and Incoherent Dihydrogen Exchange. In this section we treat the various exchange processes of Figure 2 using methods of formal kinetics. We are interested in conditions under which these reactions can be described in terms of a single phenomenological complex rate constant $k + i\pi J$ characterizing the interconversion between A and A′. We assume that the interconversion between the ground states and the intermediate states B and B′ is incoherent and characterized by the rate constants k_{AB} and k_{BA}. In the case of identical particles, i.e., the pairs HH or DD, the exchange between B and B′ will be a coherent tunnel process, characterized by the exchange J_B. On the other hand, J_B will be zero in the case of a HD pair which may, however, be subject to an incoherent exchange between B and B′, characterized by the rate constant k_{BB}. This process corresponds to an incoherent tunneling process if B and B′ are located below the top of the barrier. In addition to the scheme of Figure 2, we may add direct contributions between A and A′, characterized by k_{AA} and J_A, for the HD and the HH and DD pairs, respectively. The mechanism of Figure 2b can be included by introducing the probability p_{AB} of particle exchange during the interconversion between A and B. $p_{AB} = 0$ for the mechanism of Figure 2a and $p_{AB} = 0.5$ for the mechanism of Figure 2b. We note that the mechanism of Figure 2c corresponds to the high-temperature reaction channel of both low-temperature mechanisms of Figure 2 (parts a and b), i.e., these cases can only be distinguished when the energies of B and B′ are lower than the energy barrier of the exchange.

All cases can be described in a combined way by the following set of coupled linear differential equations for the time dependence of the mole fractions x_i

$$\frac{\mathrm{d}}{\mathrm{d}t}\begin{pmatrix} x_A \\ x_B \\ x_{B'} \\ x_{A'} \end{pmatrix} = \begin{pmatrix} -k_{AA} - k_{AB} - i\pi J_A & (1-p_{AB})k_{BA} & p_{AB}k_{BA} & k_{AA} + i\pi J_A \\ (1-p_{AB})k_{BA} & -k_{BA} - k_{BB} - i\pi J_B & k_{BB} + iJ_B & k_{AB}p_{AB} \\ k_{AB}p_{AB} & k_{BB} + i\pi J_B & -k_{BA} - k_{BB} - i\pi J_B & (1-p_{AB})k_{BA} \\ k_{AA} + i\pi J_A & p_{AB}k_{BA} & (1-p_{AB})k_{BA} & -k_{AA} - k_{AB} - i\pi J_A \end{pmatrix} \begin{pmatrix} x_A \\ x_B \\ x_{B'} \\ x_{A'} \end{pmatrix} \tag{1}$$

This set has no simple general analytical solution. However, assuming that the concentration of B is small, i.e., $x_A(t) + x_{A'}(t) = 1 - x_B(t) - x_{B'}(t) \approx 1$ the steady state conditions $\mathrm{d}x_B/\mathrm{d}t = \mathrm{d}x_{B'}/\mathrm{d}t = 0$ is valid and eq 1 simplifies to

$$\frac{\mathrm{d}}{\mathrm{d}t}\begin{pmatrix} x_A \\ x_{A'} \end{pmatrix} = \left(\begin{array}{c|c} -k - i\pi J & k + i\pi J \\ \hline k + i\pi J & -k - i\pi J \end{array}\right)\begin{pmatrix} x_A \\ x_{A'} \end{pmatrix} \tag{2}$$

with the solution

$$x_A(t) = {}^1/_2 + (x_A(0) - {}^1/_2)\exp(-2(k + i\pi J)t),$$
$$x_{A'}(t) = {}^1/_2 + (x_{A'}(0) - {}^1/_2)\exp(-2(k + i\pi J)t) \tag{3}$$

k represents an average rate constant of the incoherent exchange between A and A′ and is given by

$$k = k_{AA} + \frac{k_{AB}}{(k_{BA} + 2k_{BB})^2 + 4\pi^2 J_B^2}(2\pi^2 J_B^2 + (k_{BA} + 2k_{BB})(2p_{AB}(1-p_{AB})k_{BA} + k_{BB})) \tag{4}$$

$$\pi J = \pi J_A + \frac{k_{AB}k_{BA}(2p_{AB} - 1)^2}{(k_{BA} + 2k_{BB})^2 + 4\pi^2 J_B^2}\pi J_B$$

where the second terms represent the contribution of B and B′. In the following, we are especially interested in these contribu-

tions to the coherent exchange between A and A′ via B and B′. Therefore, we set $\pi J_A = k_{AA} = 0$ in order to discuss the different cases of Figure 2a.

Firstly, we note that in the case of Figure 2b—where the probability of the formation of B and of B′ is each $p_{AB} = {}^1/_2$ for all pair combinations HH, HD, and DD it follows that

$$k = k_{AB}/2,\ \pi J = 0 \tag{5}$$

Thus, even if there were a coherent exchange between B and B′ it could not contribute to the average coherent exchange. k is determined by the rate constant of activation from A to B. The factor ${}^1/_2$ arises from the fact that only half of the activation processes also lead to an exchange. We note that the mechanism of Figure 2c also implies that $p_{AB} = {}^1/_2$. Therefore, in this case it is also clear that the rotation in B will not influence either k or J.

For the case of a HD pair (Figure 2a), $J_B = 0$ and $p_{AB} = 0$, i.e., it follows that

$$k = \frac{k_{AB}k_{BB}}{k_{BA} + 2k_{BB}},\quad \pi J = 0 \tag{6}$$

with

$$k = k_{AB}/2 \text{ for } k_{BB} \gg k_{BA} \tag{6a}$$

and

$$k = k_{BB}k_{AB}/k_{BA} \approx k_{BB}(x_B/x_A) \text{ for } k_{BB} \ll k_{BA} \tag{6b}$$

Now, if the rate limiting step is the interconversion between B and B′ the latter contributes the term $k_{BB}(x_B/x_A)$ where x_B/x_A is the equilibrium constant of the activation step. On the other hand, if the activation is rate limiting we obtain the same result as in eq 5 for the case of Figure 2b. This case will be realized if B is located close to or above the top of the barrier. Then the HD pair may be a free incoherent rotor. However, as this rotation is not rate limiting, it has no influence on k.

The most important case is the exchange of an HH and a DD pair via an excited state according to Figure 2a. This case is further illustrated in Figure 3a. Now, with $k_{BB} = 0$ and $p_{AB} = 0$ and we obtain

$$k = \frac{k_{AB}}{2}\frac{1}{1 + (k_{BA}/2\pi J_B)^2},\quad \pi J = \frac{k_{AB}}{2}\frac{2\pi J_B/k_{BA}}{1 + (2\pi J_B/k_{BA})^2} \tag{7}$$

For illustration these quantities are plotted in Figure 3a as a function of the ratio $2\pi J_B k_{BA}$. As J_B increases with increasing temperature the abscissa is a nonlinear measure of the absolute temperature. In Figure 3b are plotted the logarithms of the same quantities as a function of $k_{BA}/2\pi J_B$ which is then a function of the inverse temperature. In other words, Figure 3b has the appearance of an Arrhenius diagram. In the coherent exchange regime at low temperature the coherent interconversion between B and B′ represents the rate limiting step, and the interconversion between A and B is very fast. Then, with $(2\pi J_B/k_{BA})^2 \ll 1$ and $k_{AB}/k_{BA} \approx x_B/x_A$ it follows that

$$k = (x_B/x_A)(2\pi J_B)^2/k_{BA} \approx 0,\quad \pi J = (x_B/x_A)J_B \tag{8}$$

i.e., A and A′ interconvert periodically. This result is identical to eq 19 of Scheurer et al.[12] under the condition of the restriction to the two lowest level pairs. In the incoherent exchange regime

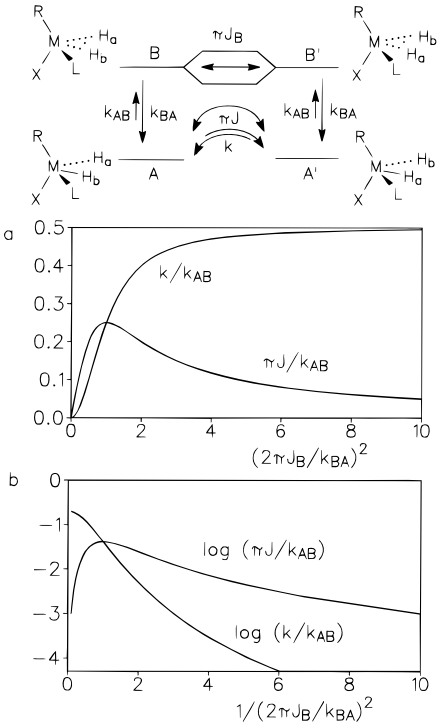

Figure 3. (a) Frequency πJ and rate constant k of the exchange between A and A′ via an incoherent activation to B and a coherent or periodic exchange between B and B′ calculated according to eq 6 as a function of $(2\pi J_B/k_{BA})^2$. (b) log πJ and log k as a function of $(k_{BA}/2\pi J_B)^2$. For further explanation see text.

$(2\pi J_B/k_{BA})^2 \gg 1$ the interconversion between A and B constitutes the rate limiting step and we obtain

$$k = k_{AB}/2,\quad \pi J = {k_{BA}}^2/4\pi J_B \approx 0 \tag{9}$$

Now, during the lifetime of the excited state B and B′ interconvert periodically very often until the system reacts either to A or to A′ with equal probabilities, and the contribution of the excited state to J becomes very small. The transition from the coherent to the incoherent regime is characterized by

$$k = \pi J = k_{AB}/4 = \pi J_B/2 \tag{10}$$

We note that eq 9 will apply in the case where B is located close or above the top of the barrier where the HH pair is a free coherent rotor. Figure 2c applies then also for this case in agreement with the result that eqs 5, 6a, and 9 give the same results. In other words, the high-temperature over-barrier mechanism of Figure 3c applies for all dihydrogen pairs HH, HD and DD, and it is no longer important whether the free rotation in the transition state is coherent or incoherent.

Finally, we note that eq 1 can easily be extended to a whole manifold of states, but the solution of this differential equation becomes more cumbersome. The two-state approach may give qualitatively good results when applied to a small temperature regime and when the population of B and B′ is small.

NMR and INS Line Shapes of Transition Metal Hydrides in the Presence of Incoherent and Coherent Dihydrogen Exchange. In this section it will be shown how J and k can be obtained using the Alexander−Binsch formalism[16] by simulation of NMR and INS line shapes of transition metal hydrides. This formalism is based on the quantum-mechanical density matrix $\rho(t)$ of the nuclear spin system of interest. Readers not familiar

with this formalism should directly proceed to a later section containing the numerical line shape calculations. The diagonal elements of the density matrix correspond to the populations of the various spin states in the environments considered. The off-diagonal elements correspond to the quantum coherences between the spin states. Single quantum coherences correspond to observable magnetization.

Equation of Motion of the Density Matrix. In a first step the Liouville von Neumann equation[16] which governs the time dependence of the density matrix must be set up, which can be written in composite Liouville-space in the form

$$\frac{d\rho(t)}{dt} = -(K + R + iL)(\rho(t) - \rho(\infty)) = -M(\rho(t) - \rho(\infty)) \tag{11}$$

K is an operator describing the molecular kinetics in terms of phenomenological rate constants and L the Liouville operator in composite Liouville space. The advantage of this operator is that it allows to describe the stochastic fluctuations in the Hamiltonian caused by the incoherent kinetics—which make the Hamiltonian time dependent—in terms of an exchange between several time independent Hamiltonians as stated above. R is the Redfield relaxation super operator describing the interaction of the spin system with the bath. Under usual conditions of high resolution NMR spectroscopy R is assumed to be diagonal, and the elements are given by two phenomenological constants, i.e., the effective negative inverse longitudinal and transverse relaxation times $1/T^r_{1eff}$ and $1/T^r_{2eff} = \pi W_o{}^r$ of the environment r. $W_o{}^r$ represents the line width of a signal arising from environment r in the absence of exchange.[16] At low temperatures this approximation breaks down; in the case of a dihydrogen pair magnetic dipole relaxation caused by molecular rotational diffusion will be dominant for which the elements of R are well-known.[20] Incoherent mutual exchange of the two hydrogen atoms does not contribute to R as the dipole interaction is not sensitive to 180° jumps.

$L = L_A \oplus L_B \oplus ...$ is the Liouville super operator in composite Liouville space, which is responsible for the coherent kinetics of ρ, where each Liouvillian is constructed from its site Hamiltonian H^r and its unit operator E^r as[20a]

$$L^r = H^r \otimes E^r - E^r \otimes H^r, \quad r = \text{A, B, ...} \tag{12}$$

Neglecting anisotropic interactions, the spin Hamiltonian of an environment r containing two hydrogen nuclei in different nuclear sites i can be written as

$$H^r = \sum_i \nu^r_r I^r_{zi} + \sum_{i<j}\sum J^r_{ij} I^r_i I^r_j \tag{13}$$

where I^r_{zi} and I^r_i are the spin operators of spin i in environment r and $\nu^r_i = \gamma_i B_o(1 - \sigma^r_i)$ the Larmor frequency of the nuclear site i in environment r, σ^r_i the isotropic chemical shielding of i, and J^r_{ij} the coupling constants between i and j in r. In the case of two protons with spin $^1/_2$

$$J^r_{ij} = (J^r_{ij})_{magn} + (J^r_{ij})_{exch} \tag{14}$$

represents the sum of the usual scalar magnetic coupling and an exchange coupling, as discussed in Figure 1. We note that Zilm et al. label the exchange couplings as $-2(J^r_{ij})_{exch}$. We include here the factor -2 in $(J^r_{ij})_{exch}$ so that J^r_{ij} is positive and equal to the experimentally observed signal splitting arising from the quantum exchange.

For the case of a single hydrogen pair exchange according to Figure 2, the time dependence of the single quantum coherences can be written in the following form (see Chart 1). For the sake of clarity we neglect the direct contributions of exchange k_{AA} and J_A. The subscripts refer to the product spin states of dihydrogen $|1> = |\alpha\alpha>$, $|2> = |\alpha\beta>$, $|3> = |\beta\alpha>$, $|4> = |\beta\beta>$. Thus, in the case where the off-diagonal elements are small, eqs 15 and 16 represent the time dependence of the magnetizations of the transitions of two AX-spin systems of

Chart 1

$$\frac{d}{dt}\begin{pmatrix}\rho^A_{12}\\ \rho^A_{13}\\ \rho^B_{12}\\ \rho^B_{13}\end{pmatrix} = \begin{pmatrix} -1/T^A_{2eff} - k_{AB} + 2i\pi\nu_{2A} & 0 & k_{BA}(1-p_{AB}) & k_{BA}p_{AB} \\ 0 & -1/T^A_{2eff} - k_{AB} + 2i\pi\nu_{1A} & k_{BA}p_{AB} & k_{BA}(1-p_{AB}) \\ k_{AB}(1-p_{AB}) & k_{AB}p_{AB} & -1/T^B_{2eff} - k_{AB} - k_{BB} + 2i\pi(\nu_{2B} + J_B/2) & k_{BB} - i\pi J_B \\ k_{AB}p_{AB} & k_{AB}(1-p_{AB}) & k_{BB} - i\pi J_B & -1/T^B_{2eff} - k_{BA} - k_{BB} + 2i\pi(\nu_{1B} + J_B/2) \end{pmatrix} \begin{pmatrix}\rho^A_{12}\\ \rho^A_{13}\\ \rho^B_{12}\\ \rho^B_{13}\end{pmatrix} \tag{15}$$

$$\frac{d}{dt}\begin{pmatrix}\rho^A_{24}\\ \rho^A_{34}\\ \rho^B_{24}\\ \rho^B_{34}\end{pmatrix} = \begin{pmatrix} -1/T^A_{2eff} - k_{AB} + 2i\pi\nu_{1A} & 0 & k_{BA}(1-p_{AB}) & k_{BA}p_{AB} \\ 0 & -1/T^A_{2eff} - k_{AB} + 2i\pi\nu_{2A} & k_{BA}p_{AB} & k_{BA}(1-p_{AB}) \\ k_{AB}(1-p_{AB}) & k_{AB}p_{AB} & -1/T^B_{2eff} - k_{AB} - k_{BB} + 2i\pi(\nu_{1B} - J_B/2) & k_{BB} + i\pi J_B \\ k_{AB}p_{AB} & k_{AB}(1-p_{AB}) & k_{BB} + i\pi J_B & -1/T^B_{2eff} - k_{BA} - k_{BB} + 2i\pi(\nu_{2B} - J_B/2) \end{pmatrix} \begin{pmatrix}\rho^A_{24}\\ \rho^A_{34}\\ \rho^B_{24}\\ \rho^B_{34}\end{pmatrix} \tag{16}$$

environments A and B, e.g., an element like ρ^A_{34} corresponds to the transition between $|\beta\alpha>$ and $|\beta\beta>$ in the environment A. In the case where all nondiagonal elements of the matrices in eqs 15 and 16 are small, the diagonal elements characterize the transitions of a usual AX-spin systems, where the real part describes the line widths and the imaginary part the line frequencies.

Equations 15 and 16 could also have been formulated in the basis consisting of the nuclear singlet state

$$|3> = |S> = (1/\sqrt{2})|\ \alpha\beta\text{-}\beta\alpha> \tag{17}$$

and the nuclear triplet states

$$|1> = |T_+>=|\alpha\alpha>,\quad |2> = |T_o>= (1/\sqrt{2})|\alpha\beta+\beta\alpha>,\quad |4> = |T>= |\beta\beta> \tag{18}$$

This basis is appropriate when the coupling constants are much larger than the chemical shift difference. Let us assume that this is the case for environment B. The transformation into the symmetrized basis is straightforward. In this case we obtain the single quantum coherences between the triplet states

$$\rho'^B_{T_+T_0} = \rho'^B_{12} = (\rho^B_{12} + \rho^B_{13})/\sqrt{2} \tag{19}$$

$$\rho'^B_{T_0T_-}1 = \rho'^B_{24} = (\rho^B_{24} + \rho^B_{34})/\sqrt{2} \tag{20}$$

and between triplet states and the singlet state

$$\rho'^B_{T_+S} = \rho'^B_{13} = (\rho^B_{12} - \rho^B_{13})/\sqrt{2} \tag{21}$$

$$\rho'^B_{ST_0} = \rho'^B_{34} = (\rho^B_{24} - \rho^B_{34})/\sqrt{2} \tag{22}$$

$$\rho'^B_{12} = (\rho^B_{12} + \rho^B_{13})/\sqrt{2}\quad \rho'^B_{13} = (\rho^B_{12} - \rho^B_{13})/\sqrt{2} \tag{23}$$

We then obtain eqs 24 and 25 (see Chart 2). As can be seen for the ρ'^B_{34} element, which represents the quantum coherence between the singlet S and the triplet T_o state in environment B, the self exchange k_{BB} adds to the relaxation rate $1/T^B_{2eff}$ to give an effective phase relaxation rate $1/T_2^{ST}$ for the coherence between the singlet and triplet states of B, i.e.

$$(1/T^{ST})_B = 1/T_{2eff} + 2k_{BB} \tag{26}$$

which should, however, not be confused with the very small rate of the forbidden spin conversion. Moreover, when $p_{AB} = 0.5$ the off-diagonal elements connecting the singlet−triplet coherence in B with the coherences of A vanish, and B cannot contribute to an average exchange coupling.

We note that in the case where the steady state approximation for the environment B applies as assumed in the previous section, eqs 24 and 25 reduce to those of a single average environment, i.e.

$$\frac{d}{dt}\begin{pmatrix}\rho_{12}\\ \rho_{13}\end{pmatrix} = \begin{pmatrix}-1/T_{2eff} - k + 2i\pi(\nu_2 + J/2) & k - i\pi J\\ k - i\pi J & -1/T_{2eff} - k + 2i\pi(\nu_1 + J/2)\end{pmatrix}\begin{pmatrix}\rho_{12}\\ \rho_{13}\end{pmatrix} \tag{27}$$

and

$$\frac{d}{dt}\begin{pmatrix}\rho_{24}\\ \rho_{34}\end{pmatrix} = \begin{pmatrix}-1/T_{2eff} - k + 2i\pi(\nu_2 - J/2) & k + i\pi J\\ k + i\pi J & -1/T_{2eff} - k + 2i\pi(\nu_1 + J/2)\end{pmatrix}\begin{pmatrix}\rho_{24}\\ \rho_{34}\end{pmatrix} \tag{28}$$

where k and J are given in eqs 4 and 5.

Finally, we are interested in the motion of the nuclear spin density matrix of dihydrogen in the absence of a magnetic field. In this case all triplet states are degenerate, i.e. $T = T_1$, T_0, T_{-1} and only a single quantum coherence between the triplet state T and the singlet state S is defined. The time dependence of the density matrix is then given by

Chart 2

$$\frac{d}{dt}\begin{pmatrix}\rho^A_{12}\\ \rho^A_{13}\\ \rho'^B_{12}\\ \rho'^B_{13}\end{pmatrix} = \begin{pmatrix}-1/T^A_{2eff} - k_{AB} + 2i\pi\nu^A_2 & 0 & k_{BA}/\sqrt{2} & (1-2p_{AB})k_{BA}/\sqrt{2}\\ 0 & -1/T^A_{2eff} - k_{AB} + 2i\pi\nu^A_1 & k_{BA}\sqrt{2} & -(1-2p_{AB})k_{BA}/\sqrt{2}\\ k_{AB}\sqrt{2} & k_{AB}\sqrt{2} & -1/T^B_{2eff} - k_{BA} + i\pi(\nu^B_1 + \nu^B_2) & i\pi(\nu^B_2 - \nu^B_1)\\ (1-2p_{AB})k_{BA}/\sqrt{2} & -(1-2p_{AB})k_{AB}/\sqrt{2} & i\pi(\nu^B_2 - \nu^B_1) & -1/T^B_{2eff} - k_{BA} - 2k_{BB} + i\pi(\nu^B_1 + \nu^B_2 + 2J_B)\end{pmatrix}\begin{pmatrix}\rho^A_{12}\\ \rho^A_{13}\\ \rho'^B_{12}\\ \rho'^B_{13}\end{pmatrix} \tag{24}$$

$$\frac{d}{dt}\begin{pmatrix}\rho^A_{24}\\ \rho^A_{34}\\ \rho'^B_{24}\\ \rho'^B_{34}\end{pmatrix} = \begin{pmatrix}-1/T^A_{2eff} - k_{AB} + 2i\pi\nu^A_2 & 0 & k_{BA}/\sqrt{2} & (1-2p_{AB})k_{BA}/\sqrt{2}\\ 0 & -1/T^A_{2eff} - k_{AB} + 2i\pi\nu^A_1 & k_{BA}\sqrt{2} & -(1-2p_{AB})k_{BA}/\sqrt{2}\\ k_{AB}\sqrt{2} & k_{AB}\sqrt{2} & -1/T^B_{2eff} - k_{BA} + i\pi(\nu^B_1 + \nu^B_2) & i\pi(\nu^B_2 - \nu^B_1)\\ (1-2p_{AB})k_{BA}/\sqrt{2} & -(1-2p_{AB})k_{AB}/\sqrt{2} & i\pi(\nu^B_2 - \nu^B_1) & -1/T^B_{2eff} - k_{BA} - 2k_{BB} + i\pi(\nu^B_1 + \nu^B_2 - 2J_B)\end{pmatrix}\begin{pmatrix}\rho^A_{24}\\ \rho^A_{34}\\ \rho'^B_{24}\\ \rho'^B_{34}\end{pmatrix} \tag{25}$$

$$\frac{d}{dt}\begin{pmatrix}\rho'^{A}_{ST}\\ \rho'^{B}_{ST}\end{pmatrix}= \left(\begin{array}{c|c} -1/T_{2eff}-k_{AB} & k_{BA} \\ \hline k_{AB} & -1/T_{2eff}-k_{BA}-2k_{BB}-2i\pi J_B \end{array}\right)\begin{pmatrix}\rho'^{A}_{ST}\\ \rho'^{B}_{ST}\end{pmatrix} \quad (29)$$

and

$$\frac{d}{dt}\begin{pmatrix}\rho'^{A}_{TS}\\ \rho'^{B}_{TS}\end{pmatrix}= \left(\begin{array}{c|c} -1/T_{2eff}-k_{AB} & k_{BA} \\ \hline k_{AB} & -1/T_{2eff}-k_{BA}-2k_{BB}-2i\pi J_B \end{array}\right)\begin{pmatrix}\rho'^{A}_{TS}\\ \rho'^{B}_{TS}\end{pmatrix} \quad (30)$$

In the steady state case for B it follows that

$$\frac{d\rho'_{ST}}{dt} = (-1/T_{2eff} - 2k - 2i\pi J)\rho'_{ST}, \qquad \frac{d\rho'_{TS}}{dt} = (-1/T_{2eff} - 2k + 2i\pi J)\rho'_{TS} \quad (31)$$

NMR and INS Line Shape Equation. In NMR, the observable signal corresponds to the expectation value of the lowering operator $I_- = I_x - iI_y$. In the thermal equilibrium, due to the random phase approximation, the density matrix is diagonal in the energy eigenbase and hence $<I_->\ = 0$. However by irradiating radio frequency pulses on the system, coherences can be created and ρ becomes nondiagonal and starts to evolve coherently under the influence of the spin Hamiltonian H. This time dependence of ρ leads to a time dependence of $<I_->$, the so-called free induction decay (FID). The NMR spectra are calculated by Fourier transformation of this expectation value. Expressing the density matrix in the Zeeman product spin basis the equation for the NMR signal is given by

$$<I_-(t)> = I_-\rho(t) = \rho^A_{12} + \rho^A_{13} + \rho^A_{24} + \rho^A_{34} + \rho^B_{12} + \rho^B_{13} + \rho^B_{24} + \rho^B_{34} \quad (32)$$

or in the case of a single averaged environment by

$$<I_->\ = \rho_{12} + \rho_{13} + \rho_{24} + \rho_{34} \quad (33)$$

In scattering experiments like INS however, in general the sample is continuously irradiated and the spectrum is directly observed. As was shown for the NMR case by Ernst and Anderson[21] both spectra are identical in the linear response regime. This equivalence between time domain and frequency domain spectra as a consequence of linear response theory is discussed in some detail by Slichter.[20c] This result from NMR can directly be applied to the INS case, with the consequence, that instead of calculating the spectra in the frequency domain, it is also possible to calculate the time evolution of the relevant detection operator and Fourier transform this time evolution to obtain the INS spectra.

In INS the observables are the expectation values of the lowering scattering operator X_- and rising scattering operator X_+, which correspond to the energy gain transitions and the energy loss transitions.[19] INS does not have the selection rules of NMR and transitions between states of different symmetry are allowed. The INS line shape equation can be expressed as

$$<X_+> = X_+\rho', \quad <X_->\ = X_-\rho' \quad (34)$$

Here, ρ' represents the density matrix in zero field where the nuclear spin symmetry basis is more appropriate. We obtain for the scattering operators in Hilbert space

$$X_- = |S><T_+| + |S><T_o| + |S><T_-| \quad (35)$$

$$X_+ = |T_+><S| + |T_o><S| + |T_-><S| \quad (36)$$

and for their expectation values

$$<X_->\ = \rho'^{A}_{TS} + \rho'^{B}_{TS}, \quad \rho'^{n}_{TS} = \rho'^{n}_{13} + \rho'^{n}_{23} + \rho'^{n}_{43}, \quad \rho'^{n}_{13} = \rho'^{n}_{23} = \rho'^{n}_{43}, \quad n = \text{A, B} \quad (37)$$

$$<X_+>\ = \rho'^{A}_{ST} + \rho'^{B}_{ST}, \quad \rho'^{n}_{ST} = \rho'^{n}_{31} + \rho'^{n}_{32} + \rho'^{n}_{34}, \quad \rho'^{n}_{31} = \rho'^{n}_{32} = \rho'^{n}_{34}, \quad n = \text{A, B} \quad (38)$$

Again, in the case of a single environment or the steady state case for B one obtains

$$<X_->\ = \rho'_{ST} = \rho'_{13} + \rho'_{23} + \rho'_{43}, \qquad <X_+>\ = \rho'_{TS} = \rho'_{31} + \rho'_{32} + \rho'_{34} \quad (39)$$

where the time dependence of ρ'_{ST} and ρ'_{TS} is given by eq 31. After Fourier transformation two Lorentzian lines appear at $-J$ and $+J$, where the line width W is given by

$$\pi W = 2k + \pi W_o, \pi W_o = 1/T_{2eff} \quad (40)$$

We note that eq 39 depends on the populations of the singlet and the triplet states which will be generally taken as parameters of the line shape analysis.

Numerical NMR and INS Line Shape Calculations. The influence of the rate constant k of the incoherent and frequency J of the coherent dihydrogen exchange on the NMR and INS line shapes are illustrated in the top row of Figure 4. In the bottom row are depicted schematically the corresponding energy level diagrams. Let us first discuss the case where $J > 0$ and $k = 0$. The calculated INS spectra are shown at the bottom of Figure 4a; the inelastic scattered lines appear at $-J$ and $+J$ with respect to the elastic peak and correspond to the singlet−triplet and the triplet−singlet transitions (Figure 4d). The relative intensity of both transitions depends on the populations x_S and x_T of the singlet and the triplet states which can be calculated in a similar way as in the case of free dihydrogen.[26a] The line intensities in Figure 4a are arbitrary and indicate that changes with temperature are expected in the case where spin conversion is fast enough to equilibrate triplet and singlet states.

When a magnetic field is turned on and an NMR experiment performed, only a single line is observed (Figure 4b, bottom) corresponding to the transitions ν_{12} and ν_{24} within the triplet states (Figure 4e). Such a spin system is normally called an A_2 type system. When the magnetic field becomes very strong and the two hydrogen sites are characterized by two different chemical shifts ν_1 and ν_2, a typical AX spin system is obtained when $|\nu_1-\nu_2| \gg J$ as depicted at the bottom of Figure 4c and

(20) (a) Ernst, R. R.; Bodenhausen, G.; Wokaun, A., *Principles of NMR in One and Two Dimensions*; Clarendon Press: Oxford, 1987. (b) Abragam, A. *Principles of Nuclear Magnetism*; Clarendeon Press: Oxford, 1961; Chapter VII. (c) Slichter C. P. *Principles of Magnetic Resonance*, 3rd ed.; Springer: Berlin-Heidelberg-New York, 1990.

(21) Ernst, R. R.; Anderson, W.A. *Rev. Sci. Instr.* **1966,** *37,* 93.

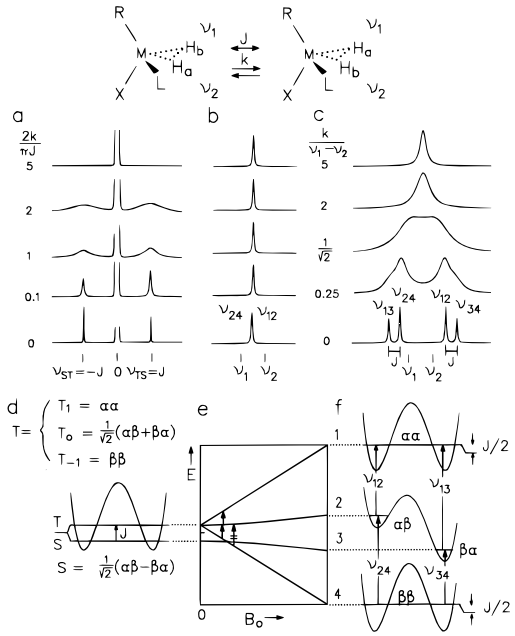

Figure 4. (a) Calculated INS spectra at $B_o = 0$ and constant values of $J = J_{magn} + J_{exch}$ but increasing rate constant k of the incoherent exchange. (b) Calculated ^{1}H NMR spectra at small values of B_o where the dihydrogen pair forms an A_2 spin system. (c) Calculated ^{1}H NMR spectra at large values of B_o where the dihydrogen pair forms an AB or AX spin system. (d) Lowest states of a quantum dihydrogen rotor at $B_o = 0$. (e) Energy level diagram as a function of B_o, where $E_{1,4} = \pm(\nu_1|2 + \nu_2|2) + J/2$, and $E_{2,3} = {}^1/_2[\pm\{(\nu_1-\nu_2)^2 + J^2\}^{1/2}]$, and the chemical shifts $\nu_i = \gamma_i B_o(1-\sigma_i)$. (f) Energy level diagram (schematically) at $B_o \gg 0$ represents the average sum of the exchange coupling.

in Figure 4f. The spectrum consists of two doublets ν_1 and ν_2 split by J. If $|\nu_1-\nu_2| \approx J$ a typical AB system arises, where the inner lines are more intense than the outer lines. In the AX limit the nuclear spin states are simply given by $|\alpha\alpha>$, $|\alpha\beta>$, $|\alpha\alpha>$, and $|\beta\beta>$ as depicted in Figure 4f. Whereas $|\alpha\alpha>$and $|\beta\beta>$ are delocalized states exhibiting the perturbation by $J/2$, $|\alpha\beta>$ and $|\beta\alpha>$ are now localized states. The nuclear spin transitions observed by NMR therefore correspond to transitions between delocalized and localized states and carry information about J. We note that in Figure 4 only the nuclear spin states are listed as usual in NMR. For the interested reader we list in the Appendix the full wave functions satisfying the Pauli exclusion principle.

As depicted in Figure 4c, the increase of k leads to line-broadening and coalescence as the chemical shifts are averaged by the incoherent dihydrogen exchange. By contrast, in the case of the A_2 spin system of Figure 4b the single line at $\nu_{12} = \nu_{24} = (\nu_1 + \nu_2)/2$ is no longer affected by k. Thus, the strong coherent dihydrogen exchange regime where $|\nu_1-\nu_2| \ll J$ of Figure 4b and the fast incoherent exchange regime where $|\nu_1-\nu_2| \ll k/\pi$ (top of Figure 4c) cannot easily be distinguished by NMR line shape analysis. In this case it is convenient to suppress J by substituting one H for D leading to two signals at ν_1 and ν_2 when the incoherent exchange is slow.[8b]

The simulations of the INS line shapes of Figure 4a now predict a broadening of the two inelastic lines given by $2k + W_0$, as predicted by eq 40. Thus, when k increases monotonously with increasing temperature this simple model predicts the INS lines to broaden until they disappear.

Experimental Results

A Multinuclear NMR Study of $(C_5Me_5)RuH_3(PCy_3)$ (1) and Its Deuterated Analogs Including HH/HD/DD Isotope Effects of the Incoherent Exchange.

The results of the dynamic NMR study of **1** are depicted in Figures 5−8 and are assembled in Tables 1−4.

As the hydride sites 1 and 3 in **1** and its deuterated analogs are equivalent the ^{1}H NMR line shapes of **1** depend only on the rate constant $k^{HH} = k_{12}{}^{HH} = k_{23}{}^{HH}$, those of **1-*d*** on k^{HH} and on $k^{HD} = k_{12}{}^{HD} = k_{23}{}^{HD}$, and those of **1-*d*$_2$** only on k^{HD}. The rate constants $k^{DD} = k_{12}{}^{DD} = k_{23}{}^{DD}$ of **1-*d*$_2$** and of **1-*d*$_3$** influence only the ^{2}H NMR spectra.

In Figure 5 are depicted the superimposed experimental and calculated ^{1}H NMR hydride signals of **1** dissolved in tetrahydrofuran-d_8. As described previously,[5c] at low temperatures site 2 exhibits a triplet splitting characterized by a temperature dependent exchange coupling constant $J_{12} = J_{23}$. A coupling constant J_{24} with the ^{31}P nucleus in site 4 cannot be resolved.

Table 1. Parameters of the ^{1}H NMR Line Shape Analyses at 500 MHz of $(C_5Me_5)RuH_3(PCy_3)$ (**1**) Dissolved in Tetrahydrofuran-d_8[a]

T/K	ν_1/Hz	ν_2/Hz	W_o/Hz	J_{12}/Hz	$k_{12}{}^{HH}/s^{-1}$
167	−5620	−6084	20	40	
177	−5625	−6087	12	48	
187	−5626	−6072	10	58	
197	−5628	−6066	8	71	
207	−5628	−6060	8	91	
217	−5628	−6055	5	115	20
227	−5630	−6052	5	145	80
237	−5632	−6045	5	170	250
247	−5635	−6035	5	179[b]	700
257	−5635	−6030	5	205[b]	1800
267	−5640	−6025	5	232[b]	4000
277	−5635	−6025	5	261[b]	10000
287	−5645	−6025	5	290[b]	50000
297	−5645	−6025	5	321[b]	≈90000

[a] Scalar coupling constant $J_{14}(H-P) = 31$ Hz. [b] Extrapolated from low temperatures.

Table 2. Parameters of the 202.4 MHz ^{31}P NMR Line Shape Analyses of $(C_5Me_5)RuH_3(PCy_3)$ (**1**) Dissolved in Tetrahydrofuran-d_8

T/K	ν_4/Hz	W_o/Hz	J_{12}/Hz	$k_{12}{}^{HH}/s^{-1}$
185	16346	11	58	
195	16354	11	71	
206	16362	11	91	
216	16372	11	115	18
226	16383	8	145	110
237	16393	8	170	300
256	16417	8	205[a]	1800
276	16440	8	261[a]	10000
296	16468	8	321[a]	≈90000

[a] Extrapolated from low temperatures.

Table 3. Parameters of the 500 MHz ^{1}H NMR Line Shape Analyses of $(C_5Me_5)RuH_2D(PCy_3)$ (**1-*d***) and $(C_5Me_5)RuHD_2(PCy_3)$ (**1-*d*$_2$**) Dissolved in Tetrahydrofuran-d_8

T/K	ν_1/Hz	ν_2/Hz	W_o/Hz	J_{12}/s^{-1} (**1-*d***)	$k_{12}{}^{HD}/s^{-1}$ (**1-*d*$_2$**)
172	−5639	−6120	8	50	
181	−5642	−6119	8	60	
192	−5640	−6113	8	78	
202	−5644	−6106	8	95	
213	−5644	−6100	5	117	10
223	−5644	−6095	5	150	50
234	−5650	−6095	5	176[a]	180
245	−5650	−6060	5	206[a]	540
255	−5645	−6060	5	234[a]	1400
265	−5650	−6060	5	264[a]	3000
275	−5650	−6060	5	295[a]	6500
287	−5650	−6060	5	333[a]	20000

[a] Extrapolated from low temperatures.

Table 4. Parameters of the 76.8 MHz ^{2}H NMR Line Shape Analyses of $(C_5Me_5)RuD_3(PCy_3)$ (**1-*d*$_3$**) Dissolved in Tetrahydrofuran-h_8

T/K	ν_1/Hz	ν_2/Hz	W_{o1}/Hz	W_{o2}/Hz	k_{12}^{DD}/s^{-1}
188	−855	−962	22	24	
202	−856	−926	18	19	
214	−857	−925	18	19	
224	−856	−924	10	10	60
234	−859	−924	8	10	180
244	−858	−924	3	10	500
257	−858	−924	3	10	800
267	−857	−9024	3	10	1700
292	−856	−924	3	10	

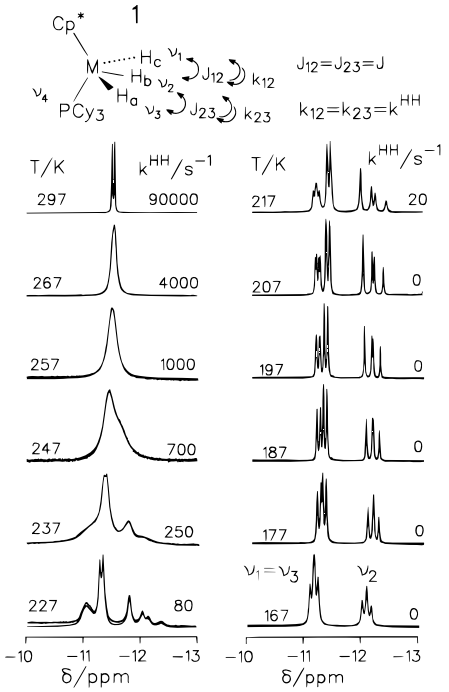

Figure 5. Superposed temperature dependent experimental and calculated 500 MHz ^{1}H NMR hydride signals of $(C_5Me_5)RuH_3(PCy_3)$ (Cy = cyclohexyl) (**1**) dissolved in tetrahydrofuran-d_8.

Sites 1 and 3 are equivalent and exhibit the expected doublet splitting with the nucleus in site 2, as $J_{12} = J_{23}$. Each line component is furthermore split by scalar coupling with the ^{31}P nucleus in site 4 with $J_{14} = J_{34} = 32$ Hz. In contrast to J_{14}, corresponding to a magnetic coupling, J_{12} represents an exchange coupling which increases strongly with temperature as revealed by the typical AB_2X signal pattern. Above 210 K, line broadening and coalescence occurs eventually leading to a doublet with an average splitting of $J(^1H-^{31}P) = (J_{14} + J_{24} + J_{34})/3 = 22$ Hz. This splitting indicates that the classical exchange process observed is purely intramolecular. By line shape analysis the exchange coupling constants J_{12} and the rate constants k^{HH} of the classical exchange are obtained.

It is remarkable and so far not recognized that in principle a heteronucleus like ^{31}P can be used in order to distinguish indirectly between the strong coherent and incoherent dihydrogen exchange regimes as the phosphorus nucleus is part of the strongly coupled AB_2X spin system. Therefore, we measured the ^{31}P NMR spectra of **1** dissolved in THF-d_8 as a function of temperature, by selectively decoupling the protons in the carbon sites. The resulting superimposed experimental and calculated ^{31}P NMR are depicted in Figure 6. Only the ^{31}P NMR chemical shift ν_4 had to be adapted as all other parameters were already

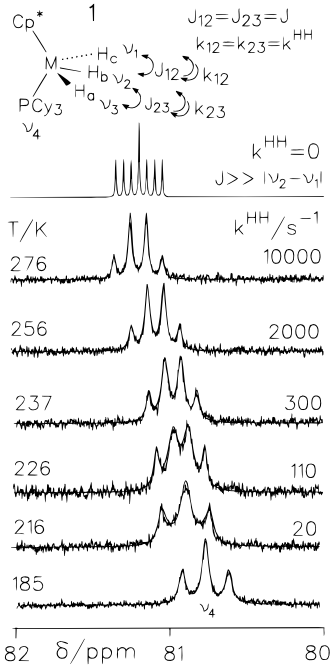

Figure 6. Superposed temperature dependent experimental and calculated 202.4 MHz ^{31}P NMR signals of **1** dissolved in tetrahydrofuran-d_8. Scalar coupling to the protons in the carbon sites was removed by selectively irradiating the aliphatic proton signals. Top spectrum: calculated for the case of a very large coupling constant J.

known by the analysis of the ^{1}H NMR spectra of Figure 5. As $J_{14} = 31$ Hz and $J_{24} \approx 0$ we observe at low temperature the expected triplet splitting. In this region J_{12} is much smaller than the chemical shift difference $|\nu_1-\nu_2|$ and high order effects are absent. As temperature is increased both J and k increase. However, the incoherent exchange dominates the spectrum leading to a transition from the triplet at low temperatures to a quartet at high temperatures as shown in Figure 6 indicating that now all three hydride nuclei are magnetically equivalent. Only small values of k of the order of J_{14} are needed for this transition to occur. For comparison we have included at the top of Figure 6 a spectrum calculated for the case where $k = 0$ but $J_{12} \gg |\nu_1-\nu_2|$. Then, a high order ^{31}P NMR signal pattern is expected consisting of seven lines equally separated by $J_{14}/6$, where the outer lines exhibit equal intensities corresponding to $^1/_2$ of the intensity of the center line.

In order to evaluate the kinetic hydrogen/deuterium isotope effects of the classical exchange processes we have analyzed the NMR line shapes of the various isotopologs of **1**. In Figure 7 are shown the superimposed calculated and experimental hydride ^{1}H NMR signals of a mixture of **1-*d*** and **1-*d*$_2$**, present in a ratio of about 1:5.6. Although the exchange couplings J_{12} for **1-*d*** could be determined at low temperature, the rate constants of this species could not be obtained because of its low mole fraction and the dominance of **1-*d*$_2$**. The latter does not exhibit exchange couplings; however, the rate constants k^{HD} could be determined for this species. As in the case of **1** the coalescence region is around 240 K. The agreement between the experimental and calculated spectra is very satisfactory.

Finally, we performed ^{2}H NMR experiments on a sample of **1-*d*$_3$** dissolved in tetrahydrofuran-h_8 in order to measure the rate constants k^{DD}. The resulting superimposed experimental and calculated ^{2}H NMR signals are shown in Figure 8. **1-*d*** and **1-*d*$_2$** could not be detected. At 189 K we observe two signals in a 2:1 ratio caused by equivalent deuterons in sites 1 and 3

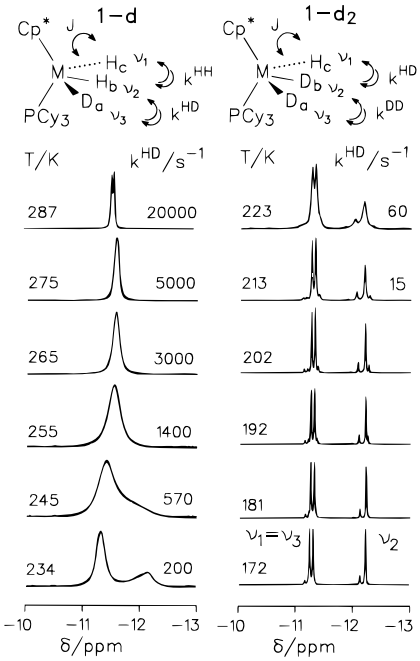

Figure 7. Superposed temperature dependent experimental and calculated 500 MHz ^{1}H NMR hydride signals of a mixture of (C_5-Me_5)$RuHD_2(PCy_3)$ **1-*d*** (15%) and (C_5Me_5)$RuH_2D(PCy_3)$ (**1-*d*$_2$**) (85%) dissolved in tetrahydrofuran-d_8.

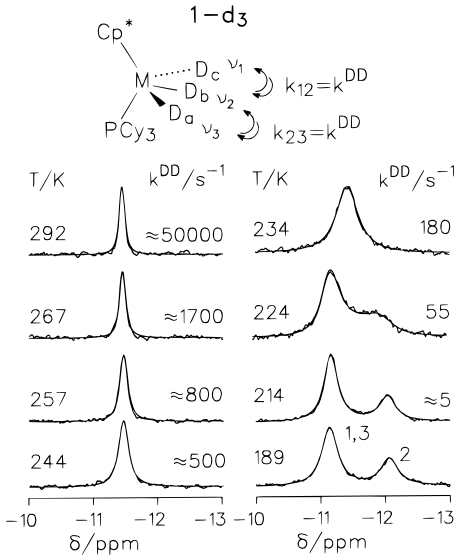

Figure 8. Superposed temperature dependent experimental and calculated 76.8 MHz ^{2}H NMR hydride signals of (C_5Me_5)$RuD_3(PCy_3)$ (**1-*d*$_3$**) dissolved in tetrahydrofuran-h_8.

and the third deuteron in position 2. When the temperature is increased, the two signals broaden and coalesce at 234 K into a single line which further sharpens with increasing temperature. Unfortunately, the line width W_o in the absence of exchange is strongly affected by transverse temperature dependent quadrupole relaxation; the rate constants included in Figure 8 and Table 4 are, therefore, subject to a large systematic error. Therefore we did not calculate the activation energy of the classical deuterium exchange. The error is smaller around the coalescence point where we obtain $k^{DD}(234\ K) = 180\ s^{-1}$. The corresponding extrapolated values for **1** are $k^{HH}(234\ K) = 163\ s^{-1}$ and for **1-*d*$_2$** $k^{HD}(234\ K) = 174\ s^{-1}$ and indicate that the isotope effects on the classical exchange processes are negligible within the margin of error.

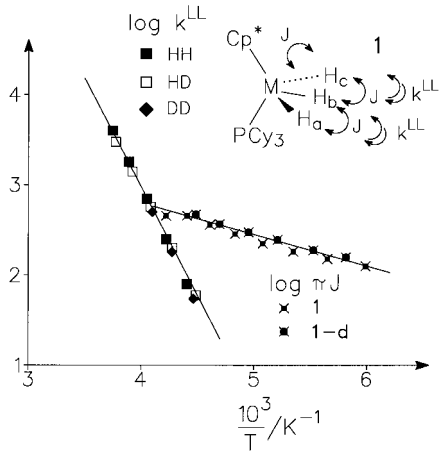

Figure 9. Arrhenius diagram of the coherent (log J_{12}) and incoherent (log k_{12}^{LL}) exchange between the inner and outer hydrons protons of **1** as a function of the inverse temperature.

A summary of all results is contained in the Arrhenius diagram of Figure 9 which includes the temperature dependent logarithmic values of πJ of the coherent HH-exchange, and the rate constants k^{HH}, k^{HD}, and k^{DD} of the incoherent exchange as a function of the inverse temperature. Within the margin of error the exchange couplings in **1** and **1-*d*** coincide, and their temperature dependence can be represented by

$$\pi J = 10^{4.3}\exp(-7.1\ \text{kJmol}^{-1}/RT)\ \text{s}^{-1}, \quad 220\ \text{K} < T < 280\ \text{K}, \quad J(240\text{K}) = 181\ \text{Hz} \quad (41)$$

In addition, Figure 9 shows that there are no kinetic HH/HD/DD isotope effects within the margin of error, i.e., the temperature dependence of the isotopic rate constants could be fitted by a single Arrhenius curve

$$k^{LL} = 10^{12.6}\exp(-46\ \text{kJ mol}^{-1}/RT)\ \text{s}^{-1}, \quad 220\ \text{K} < T < 280\ \text{K}, \quad k^{LL}(240\ \text{K}) = 330\ \text{s}^{-1}, \quad \text{LL} = \text{HH, HD, DD} \quad (42)$$

The INS Spectra of W(PCy)$_3$(CO)$_3$(η-H$_2$). As an experimental example of an INS line shape analysis using the Alexander−Binsch formalism we have analyzed the INS spectra of the tungsten dihydrogen complex,[2] some of which have been described previously.[3e] Here we simulated the line shape associated with the two rotational tunnel transitions of **2** as a function of the parameters J and k. J determines the line positions. Some typical superimposed experimental and calculated spectra are depicted in Figure 10, where for the sake of clarity plots of the calculated line shapes of the outer rotational tunnel transitions of **1** without the contribution of the quasielastic center line are included. J increases only slightly with increasing temperature, in contrast to the Lorentzian line widths W which increases strongly. In other words, the lines broaden with increasing temperature until they disappear. We note that the relative intensity of the singlet−triplet and the triplet−singlet transitions are almost the same in the whole temperature range covered, in contrast to the case of a thermal equilibrium between the singlet and the triplet states. This indicates that the singlet−triplet conversion rates are very slow in the sample measured and that the actual relative intensity of the two peaks is arbitrary depending on the history of the sample.

According to eq 40 the Lorentzian INS line width can be written as $\pi W = \pi W_o + 2k + 2k_o$, where W_o represents the contribution arising from other sources than the dihydrogen

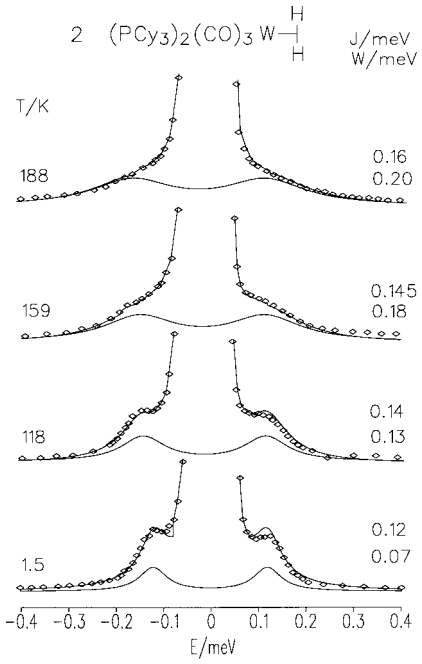

Figure 10. Superposed experimental and calculated INS spectra of $W(PCy)_2(CO)_3$ (η-H_2) (**2**) as function of temperature. Some of the spectra were previously reported in ref 3e. *W* is the total line width in meV; *J* is the rotational tunnel splitting in meV (1 meV = 2.318×10^{11} Hz = 8.065 cm^{-1}). For further explanation see text.

Table 5. Parameters of the INS Line Shape Analyses of Solid $W(PCy)_3(CO)_3$ (η-H_2) (**2**)

T/K	*J*/meV	*W*/meV	k^a/s^{-1}
1.5	0.12	0.07	
29	0.135	0.08	
64	0.14	0.08	
118	0.14	0.13	$(2\pm1.5) \times 10^{10}$
159	0.145	0.18	$(4.0\pm0.6) \times 10^{10}$
189	0.16	0.20	$(4.7\pm0.6) \times 10^{10}$

[a] $k = p(W-W_0)/2$, $W_0 \approx W_{1.5K}$ represents the temperature dependent part of the incoherent exchange rate constant.

exchange, k_o accounts for a channel dominating at low temperatures, involving a very small activation energy and *k* the observable temperature dependent part of the rate constant of the incoherent dihydrogen exchange. As πW_o and k_o are difficult to separate we calculate the temperature dependent part from the equation $k = \pi(W - W_{1.5K})/2$. The values obtained including the estimated error are assembled in Table 5. A plot of log *k* vs $1/T$ is depicted in Figure 11 which includes also the pre-exponential value of $10^{12.6}$ s^{-1} reported in the previous section for **1**. It is evident that it is difficult to estimate correctly the temperature dependent term *k* at low temperatures where $k < \pi W_o/2 + k_o$. Nevertheless, by including the preexponential factor there is some evidence of a non-Arrhenius behavior of *k*. We estimate an activation energy at high temperature of about 7 kJ mol^{-1}. In Figure 11 we have also included the rotational tunnel frequency πJ. The values of the latter are larger but the temperature dependence smaller as compared to the incoherent rotation. This pattern is similar to the case of the trihydride **1** whose Arrhenius diagram was depicted in Figure 9.

Discussion

In the theoretical section we have studied using formal kinetics how various dihydrogen exchange mechanisms illustrated in Figure 2 lead to a superimposed coherent and incoherent dihydrogen exchange mechanism characterized by an average rate constant *k* and an average tunnel frequency or exchange coupling *J*. Both quantities are, in principle, closely related. If *k* and *J* are in the Hz to kHz range they can be obtained by NMR line shape analysis using the well-established Alexander−Binsch formalism, because of the possibility to include the exchange couplings in the nuclear spin Hamiltonian. The introduction of additional coupled spins can be of help to distinguish between the regimes of strong exchange coupling and fast incoherent exchange. Furthermore, the Alexander−Binsch formalism can be used to calculate the INS-rotational tunneling bands of transition metal hydrides in terms of the same parameters *k* and *J*, when the latter are in the GHz range. As experimental examples we have evaluated these parameters by multinuclear NMR line shape analysis in the case of $Cp^*RuH_3(PCy_3)$ ($Cp^* \equiv C_5(CH_3)_5$ and Cy ≡ cyclohexyl) **1** and its deuterated isotopomers dissolved in organic liquids and by INS line shape analysis in the case of the tungsten dihydrogen complex $W(PCy)_2(CO)_3$ (η-H_2). In order to further characterize the incoherent dihydrogen exchange in **1** in terms of the various mechanisms of Figure 2 the full kinetic HH/HD/DD isotope effects were reported for this process. The experimental results are contained in the Arrhenius diagrams of Figures 9 and 11.

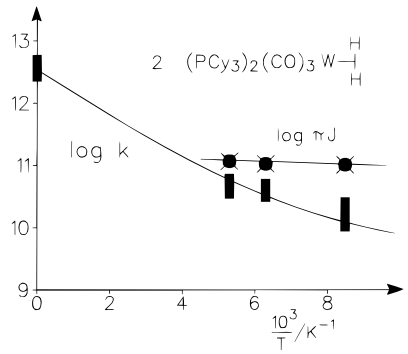

Figure 11. Arrhenius diagram of the coherent (log πJ) and the incoherent (log *k*) dihydrogen rotation in **2**. The estimated pre-exponential factor of the incoherent exchange was taken from **1**. For further explanation see text.

In the following discussion we firstly want to discuss the meaning of a superimposed coherent and incoherent dihydrogen exchange in NMR and INS and then discuss the information contained in the experimental results.

The Concept of Superimposed Coherent and Incoherent Dihydrogen Exchange. At first sight it may seem odd that the exchange between two hydrogen nuclei can at the same time be coherent and incoherent, i.e., at the same time be a periodic and an aperiodic process. However, this concept can be understood with the help of Figure 4 which depicts in the bottom row schematically the energy level diagram of two hydrogen spins as a function of the strength of a magnetic field B_o. When the field is increased, the two-spin system is converted from the A_2 to the AB and eventually to the AX type as long as the two hydrogen sites exhibit different chemical shifts. During this process the triplet spin states $|\alpha\alpha>$ and $|\beta\beta>$ remain spatially delocalized states shifted only by the Zeeman energy term. By contrast, the symmetry of the singlet state $|S>$ and the triplet state $|T_o>$ is broken in a strong field leading to the states $|\alpha\beta>$ and $|\beta\alpha>$. We note that for complete wave functions satisfying the Pauli exclusion principle (s. Appendix-)one cannot associate a particle number to the two sites. Nevertheless, the $|\alpha\beta>$ and $|\beta\alpha>$ are "localized" states in the

sense that $|\alpha\beta>$ characterizes the situation where a spin experiencing the chemical shift ν_1 is in state $|\alpha>$ and a spin experiencing ν_2 in state $|\beta>$. Therefore, in NMR one can use the nuclear spin functions alone. The indicated transitions observed in NMR (see bottom spectrum of Figure 4c) connect spatially localized states with delocalized states, and the transtion frequencies, therefore, are affected by J as illustrated schematically in Figure 4c. As a consequence, a rate process is conceivable which has the effect of exchanging the spins in the two nuclear sites, leading to an interconversion of the spin states $|\alpha\beta>$ *and* $|\beta\alpha>$, described by a rate constant $k_{\alpha\beta\rightarrow\beta\alpha} \approx k_{\beta\alpha\rightarrow\alpha\beta} \approx k$. This process exchanges the chemical shifts of the two spins according to the mechanisms of Figure 2, i.e., leads to line broadening and coalescence as indicated in Figure 4c. As two hydrogen nuclei are exchanged, one can label the rate constants k as k^{HH} and compare this value to the rate constants $k^{HD} \approx k^{DH}$ of the interconversion between the configurations HD and DH of the related isotopologs.

It is unlikely that the incoherent dihydrogen exchange is a phenomenon restricted to the presence of a magnetic field, i.e., quenched without field. In the theoretical section we therefore transformed the Alexander−Binsch equation of the two-spin system into the symmetry basis and switched the field off. As a result, the transitions between the nuclear singlet and triplet states as observed by INS were found to be broadened by the factor $W = 2k/\pi$, which explains the evolution of the INS bands in Figures 4a and Figure 10 when k, i.e., the temperature is increased.

Mechanisms of Dihydrogen Rotation. We come now to a discussion of how thermal activation of a ground state A into an excited state configuration B and or B′ as depicted schematically in Figure 2 can either lead to an internal return to A or to a coherent or incoherent exchange to A′. In the mechanism of Figure 2a B and B′ are located below the top of the barrier. Inthe case of an HD-pair B and B′ may interconvert by incoherent tunneling, characterized by the rate constant k_{BB}. As can be inferred from eq 6 of the theoretical section, assuming the steady state approximation the contribution of this mechanism to the overall incoherent exchange rate constant between A and A′ is given by $k_{AB}/2$ when the activation represents the rate limiting step, i.e., if $k_{BA} \ll k_{BB}$, and by $k_{BB}(x_B/x_A)$ when the exchange between B and B′ is rate limiting, i.e., if $k_{BA} \gg k_{BB}$. x_B/x_A represents the equilibrium constant of the formation of B from A.

This mechanism is not operative in the case of HH or DD pairs where B and B′ interconvert coherently with tunnel frequency J_B. In the theoretical section it was shown that in the case where the deactivation step from B to A is fast as compared to the coherent exchange in B ($4\pi^2 J_B^2/k_{BA}^2 \ll 1$)—i.e., the lifetime $t_B = 1/k_{AB}$ of B is short as compared to $1/2\pi J_B$—state B does not contribute to k but contributes with $\pi(x_B/x_A)J_B$ to πJ (eq 8). On the other hand, this state contributes the term $k_{AB}/2$ to k if $4\pi^2 J_B^2/k_{BA}^2 \gg 1$, i.e., if the lifetime τ_B is much longer than $1/2\pi J_B$ (eq 9). In this case many periodic dihydrogen rotations take place during the lifetime of B leading to an equal probability of internal return to A or to A′. Moreover, B does no longer contribute to the average value of J a term proportional to J_B (eq 8), but the term $k_{BA}^2/4\pi J_B \approx 0$ (eq 9). This result solves the problem of the reported numerical instability[9a−c] of the calculated values of J when the contributions of states located close or above the barrier of rotation are considered. The instability occurs because the sign of the exchange couplings J_B of these states can be positive or negative, as depicted in Figure 1a, and their absolute values can be very large. As proposed by Scheurer et al.[12] both J and k must be calculated, assuming values for the lifetimes τ_B. The expressions of eq 6 derived for the two-state exchange model of Figure 2a can then be a first rough estimate. Another consequence is that if the energy of B is located below the top or the barrier and its lifetime is long enough, the mechanism depicted in Figure 2a would lead to an incoherent tunneling pathway for the exchange between A and A′. As the coherent exchange in B is only well defined for the HH or for DD pairs, but not for HD pairs, major "symmetry induced" kinetic HH/HD/DD isotope effects are expected.

In the case of the mechanism of Figure 2b the H···H axis has rotated 90° as compared to the ground state. As the probability of a clockwise and a counterclockwise rotation are equal the formation of B and of B′ will automatically lead to an incoherent rotation, even in the case of the barrier of rotation between B and B′. Whether this rotation is coherent or incoherent does no longer matter any more. This mechanism resembles the mechanism proposed by Szymanski.[11]

Finally, in Figure 2c the formation of B is associated with a configuration involving a more or less freely rotating dihydrogen unit. This case represents in a way the high temperature over-barrier mechanism related to Figure 2 (parts a and b). Now, formation of B and the back-reaction to A or A′ are associated with a permutation of the nuclei with a probability $^1/_2$ during the interconversion between A and B, similarly as in Figure 2b. The formation of B contributes then again with $k_{AB}/2$ to k. We note that in both cases, i.e., Figure 2 (parts b and c) no symmetry induced kinetic HH/HD/DD isotope effects are expected as both mechanisms are conceivable for the isotopic HH, HD, and DD reactions. The kinetic isotope effects on the incoherent exchange may be mainly determined by the change of the zero-point energies between A and B.

So far, we have only considered a single excited state pair B and B′ where we assumed that the energy of this pair increases with increasing temperature. In Figure 12 we discuss in more detail how this assumption is justified. In Figure 12a−c are plotted schematically one-dimensional potentials of the dihydrogen motion where the barrier of rotation decreases with a decreasing HH distance. This decrease is also related to an increase of the distance between the dihydrogen center and the metal.[9] The rotational wave functions can easily be calculated by solving the Mathieu differential equation;[22]they occur in pairs split by the energy hJ_n. As some of us have noted before,[7a] the sign of J_n alternates when n is increased. In the case of a two-dimensional rotor the sign alternation is not regular but still there.[9a−c] Therefore, the incoherent "vertical" excitation in each of the configurations of Figure 12a−c as indicated by the double arrows does not lead to an increase but to a decrease of the Boltzmann average J with increasing temperature. By contrast, "horizontal" excitation of a dihydride complex according to Figure 12d populating dihydrogen-like configurations leads to an increase of J with increasing temperature.[7a] On the other hand, a typical dihydrogen complex (Figure 12e) has access to excited states with smaller or larger splittings, and the temperature dependence may be less pronounced. We note that the model of Figure 12 has been further explored[9] by *ab initio* calculations of the reaction energy surface of various hydrides. It was shown that the dihydrogen configurations correspond rather to excited vibrational states[9] rather than to metastable

(22) (a) Wallach, D.; Steele, W. A. *J. Chem. Phys.* **1976**, *52*, 2534. (b) National Bureau of Standards, *Tables relating to Mathieu functions*; Columbia University Press: New York, NY, 1951.

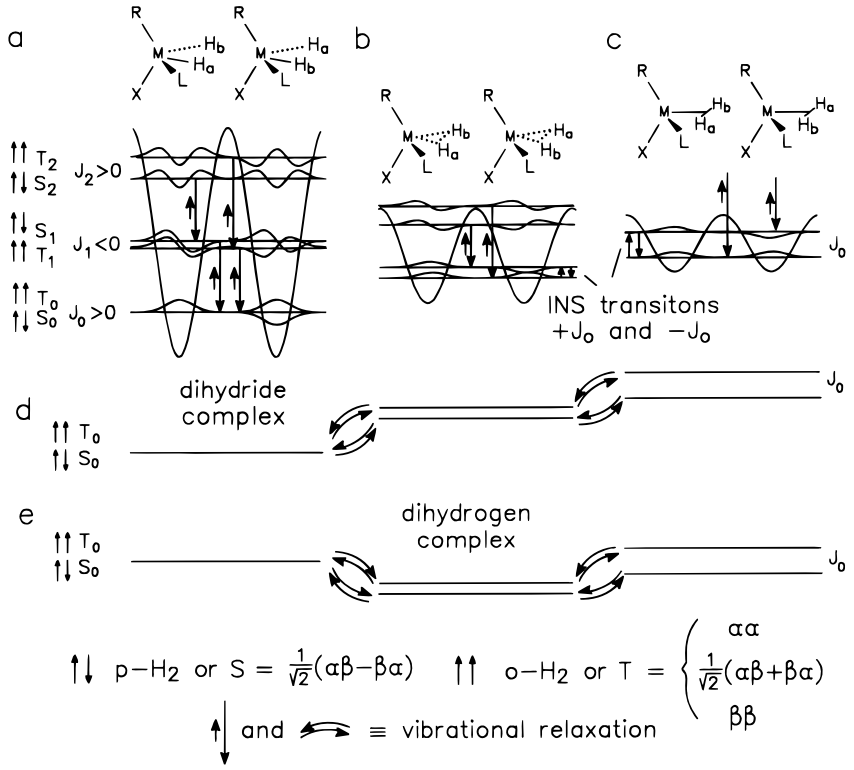

Figure 12. (a)−(c) One-dimensional potentials, energy level diagrams, and nuclear wave functions (schematically) of a hindered dihydrogen quantum rotor in a transition metal complex according to ref 7 at different fixed H···H distances. The states occur in pairs consisting of a nuclear singlet and a nuclear triplet state S_n and T_n, with the energy difference or tunnel splitting J_n. The spatial parts of S_n and of T_n are symmetric or antisymmetric with respect to a 180° rotation. For a dihydride configuration (a) the barrier is large but decreases in stretched (b) and in nonstretched dihydrogen configurations (c). In the same sequence the ground state rotational splitting J_o increases. Note that the number of state pairs n is arbitrary and may be larger than indicated. (d) and (e) More-dimensional model of a hindered dihydrogen quantum rotor with variable H···H distances. Only the two lowest state pair is shown. (d) Typical case of a dihydride complex. (e) Typical case of a dihydrogen complex.

configurations[7a] which does, however, not change the picture substantially as both vibrational states and metastable configurations interchange by rate processes. However, we note that the model of Figure 12 is only complete if one considers that levels with splittings J_n larger than the inverse vibrational lifetimes which are of the order of 10^{11} s^{-1} do not contribute to the Boltzmann average of J but to k as shown in the quantum-mechanical treatments of Szymanski[11] and Scheurer et al.[12] as discussed above.

Coherent vs Incoherent Exchange in 1 and 2. We come to a discussion of the Arrhenius diagrams of the coherent and incoherent dihydrogen exchange processes of **1** and **2**, depicted in Figures 9 and 11. Although both diagrams have been obtained by completely different methods sensitive in very different dynamic ranges similar patterns are obtained. The temperatures above which the incoherent exchange processes dominate preventing the further determination of J are around 250 K in both cases. In the case of **1** we note that within the margin of error we do not obtain significant HH/HD/DD isotope effects on the incoherent dihydrogen exchange. On the background of very large effects in other double proton transfer reactions[19] this result is not trivial and implies some important information, especially the finding that the incoherent symmetric HH and DD exchange processes exhibit similar rate constants as the incoherent HD process. In other words, there are no symmetry induced kinetic isotope effects.

The Arrhenius patterns of **1** and **2** are qualitatively reproduced by the graph of Figure 3b although this graph is based on the assumption of a single reaction channel B to B′ whose energy increases with increasing temperature, whereas for a quantitative treatment all levels have to be taken into account as proposed by Scheurer et al.[12] We note in the graph of Figure 3b that the energies of activation of log πJ and of log k vs $1/T$ are not the same although they are both caused by the same levels B and B′. This is because with increasing temperature these levels contribute more and more to k and eventually lead to a reduction of J.

In the two experimental cases of **1** and **2** we note that in both cases the activation energies determining the temperature dependence of the incoherent exchange in the high temperature regions (46 kJ mol^{-1} for **1** and about 7 kJ mol^{-1} for **2**) are substantially larger than the corresponding energies determining the temperature dependence of J (7.1 kJ mol^{-1} for **1** and ≈ 0 for **2**). We interpret these findings not in terms of Figure 3b but with different reaction channels responsible for the two kinds of exchange processes. Thus, the excited state levels determining the activation energies of the coherent exchange are lying much lower in energy as those responsible for the incoherent processes.

These findings can be rationalized in terms of the model of Figure 12. The coherent exchange in **2** is essentially determined by the molecular ground state, i.e., by a configuration of the type of Figure 12b. The tunnel splitting of 0.12 meV was shown[3e] to correspond in the one-dimensional approximation to a rotational barrier of about 762 cm^{-1} or 9 kJ mol^{-1}. The average rotational tunnel splitting does not change at higher temperatures which—in the fast vibrational exchange limit—would be consistent with an excitation to configurations exhibiting larger and smaller rotational barriers according to Figure 12e. On the other hand, as the inverse tunnel splittings and the vibrational lifetimes are almost of the same order any thermal excitation may only contribute to k alone and leave J

almost unchanged. The activation energy of the incoherent process is only 7 kJ mol^{-1} at high temperature and even smaller at lower temperatures, as was noticed already in ref 3e. This reduction of the rotational barrier is consistent with an incoherent over-barrier rotation in the right-hand configuration. The apparently smaller activation energy at lower temperatures is consistent with incoherent tunneling in lower lying states.

By contrast, in the case of **1** no temperature independent ground state rotational tunneling can be observed which must, therefore, be smaller than a few Hz. As the exchange couplings increase with temperature, their temperature dependence must be governed by excitation of the dihydrogen like configurations as indicated in Figure 12d. The observation that the pre-exponential factors of the incoherent exchange in **1** are around $10^{12.6}$ s^{-1}, which is typical for an intramolecular reaction requiring no entropy changes,[15] and the absence of kinetic HH/HD/DD isotope effects indicate that the incoherent process in this molecule refers to an over-barrier process with a height of approximately 46 kJ mol^{-1}, corresponding to the true more-dimensional barrier of rotation. At this point the zero-point energies are not very different as compared to the ground states because otherwise substantial kinetic HH/HD/DD isotope effects should be observed. The absence of a symmetry induced kinetic isotope effect indicates that the labeling of two identical particles by different spins is similar to isotopic labeling. We note, however, that substantial kinetic isotope effects may be observed if one could measure these effects at lower temperatures. In this case, both normal as well as symmetry induced kinetic isotope effects corresponding to a different reaction mechanism for the HH (or DD) rotation as compared to the HD rotation should arise. This requires either to use magnetization transfer methods in order to measure smaller rate constants at lower temperatures or the study of other systems with larger rate constants *k*.

Comparison between Transition Metal Hydrides and Chlorins. We are now able to understand why the exchange of the two protons in chlorin (Figure 1b) is not coherent. There are several reasons which can be invoked. The first reason is that the activation step consists of a 90° rotation of the proton pair to the nonprotonated nitrogen atoms, forming a second metastable tautomer. Here, the probability of a clockwise or counterclockwise rotation is $^1/_2$,[15] similar as indicated for the transition metal hydride case in Figure 2b. For this case eq 5 predicted no contribution from a possible exchange coupling in the intermediate state. On the other hand, in the case of chlorins the protons are transferred stepwise in each reaction step,[15] i.e., the situation that two nitrogen−hydrogen bonds are broken and a dihydrogen bond formed does not arise. Each elementary proton transfer involves a considerable kinetic H/D isotope effect, in contrast to the dihydrogen rotation case. This comparison, therefore, leads to the speculation that the special exchange properties of transition metal hydrides would not be realized if the molecules did not have facile access to dihydrogen configurations by excitation of anharmonic vibrational modes.

Conclusions

It has been shown that the inclusion of the quantum exchange into the nuclear spin Hamiltonian allows one to use the phenomenological NMR line shape theory of chemical exchange developed by Alexander and Binsch[16] in order to calculate not only NMR but also INS spectra of transition metal hydrides containing dihydrogen pairs subjected to coherent and incoherent exchange. Thus, this theory connects these two methods and provides a better understanding of several so far unexplained experimental observations in the area of dihydrogen mobility in the coordination sphere of transition metal hydrides. We have proposed a contribution to the line width of the INS spectra which arises from the incoherent exchange and has not yet previously been recognized. This broadening occurs in addition to other well established contributions arising from the interaction of the bound dihydrogen with phonons at elevated temperatures. A physical picture of a superimposed coherent and incoherent dihydrogen exchange mechanisms has been proposed leading to the speculation that the incoherent exchange takes place not only at energies at the top or above the rotational barrier but also below the top of the barrier via thermally activated tunneling. Such a process is conceivable without problems in the case of HD-pairs and should lead to a non-Arrhenius behavior of the rate constants of the incoherent exchange at low temperatures as well as to kinetic HH/HD/DD isotope effects in the future. Thus, studies of the incoherent processes could shed additional light also on the quantum exchange and help to solve the problem of the convergence of calculated *J* at high temperatures. Furthermore, the link between these exchange phenomena and problems of the mechanisms of hydrogenation reactions are closely related as has been shown by some of us recently.[17]

Acknowledgment. This work was supported by the Deutsche Akademische Austauschdienst, Bonn-Bad Godesberg, within the program PROCOPE, the European Union, Brussels, within the Human Capital & Mobility Network "Localization and Transfer of Hydrogen", and the Fonds der Chemischen Industrie, Frankfurt.

Appendix

In NMR the product spin functions of two spins a and b with spin $^1/_2$ systems are $|\alpha\alpha>$, $|\alpha\beta>$, $|\beta\alpha>$, and $|\beta\beta>$. The complete wave functions statisfying the Pauli-exclusion principle are given as usually by the Slater determinants

$$|\Phi_1> = 1/\sqrt{2}\begin{vmatrix} |\psi_1(a)\alpha(a)> & |\psi_2(a)\alpha(a)> \\ |\psi_1(b)\alpha(b)> & |\psi_2(b)\alpha(b)> \end{vmatrix} \rightarrow |\alpha\alpha> \quad \text{(A1)}$$

$$|\Phi_2> = 1/\sqrt{2}\begin{vmatrix} |\psi_1(a)\alpha(a)> & |\psi_2(a)\alpha(a)> \\ |\psi_1(b)\alpha(b)> & |\psi_2(b)\alpha(b)> \end{vmatrix} \rightarrow |\alpha\beta> \quad \text{(A2)}$$

$$|\Phi_3> = 1/\sqrt{2}\begin{vmatrix} |\psi_1(a)\beta(a)> & |\psi_2(a)\alpha(a)> \\ |\psi_1(b)\beta(b)> & |\psi_2(b)\alpha(b)> \end{vmatrix} \rightarrow |\beta\alpha> \quad \text{(A3)}$$

$$|\Phi_4> = 1/\sqrt{2}\begin{vmatrix} |\psi_1(a)\beta(a)> & |\psi_2(a)\beta(a)> \\ |\psi_1(b)\beta(b)> & |\psi_2(b)\beta(b)> \end{vmatrix} \rightarrow |\beta\beta> \quad \text{(A4)}$$

Terms such as $\psi_i(a)\alpha(a)$ indicate a configuration where particle *a* adopts spin state α and the spatial function ψ_i. The topology of usual molecules is such that hydrogen nuclei are confined to limited spatial regions within the molecular frame, called nuclear sites i characterized by their Larmor frequencies ν_i. In such a

(23) Limbach, H. H. Dynamic NMR Spectroscopy in the Presence of Kinetic Hydrogen Deuterium Isotope Effects. In *NMR Basic Principles and Progress*; Berlin, Heidelberg, New York, 1990; Vol. 26, Chapter 2.

(24) J_{HD} = 43 Hz: Nageswara Rao, B. D.; Anders, L. R. *Phys. Rev.* **1965**, *140*, A112−A117. (b) J_{HT} = 299 Hz: Neronov, Y. I.; Barzakh, A. E. *Zh. Eksp. Teor. Fiz.* **1977**, *72*, 1659 or *Sov. Phys. JETP* **1977**, *45*, 871.

(25) Eckert, J. Unpublished results.

(26) (a) Silvera, I. F. *Rev. Mod. Phys.* **1980**, *52*, 393. (b) Buch, V.; Devlin, J. P. *J. Chem. Phys.* **1993**, *98*, 4195. Buch, V. *J. Chem. Phys.* **1994**, *100*, 7610.

(27) Bell, R. P. *The Tunnel Effect*, 2nd ed.; Chapman and Hall: London, 1980.

point approximation $\psi_i(a)$ would then correspond to a configuration of a in site i. Φ_2 indicates that both particles a and b are with equal probabilities in both nuclear sites, but nevertheless it also indicates that site 1 always contains a particle with spin α and nuclear site 2 a particle with spin β. Therefore, Φ_2 can be simply characterized as usual in NMR only by the spin product function $|\alpha\beta>$. The symmetrized wave functions are obtained by linear combination of Φ_2 and Φ_3

$$|\Psi_1> = |\Phi_1> = 1/\sqrt{2}|(\psi_1(a)\psi_2(b)-\psi_2(a)\psi_1(b)> |\alpha(a)\alpha(a)> \rightarrow |\alpha\alpha> \equiv |T_+> \quad \text{(A5)}$$

$$|\Psi_2> = 1/\sqrt{2}|\Phi_2+\Phi_3> = 1/\sqrt{2}|(\psi_1(a)\psi_2(b)-\psi_2(a)\psi_1(b)> 1/\sqrt{2}|\alpha(a)\beta(b)+\beta(a)\alpha(b)> \rightarrow 1/\sqrt{2}>|\alpha\beta+\beta\alpha> \equiv |T_o> \quad \text{(A6)}$$

$$|\Psi_3> = 1/\sqrt{2}|\Phi_2-\Phi_3> = 1/\sqrt{2}|\psi_1(a)\psi_2(b)+\psi_2(a)\psi_1(b)> 1/\sqrt{2}|\alpha(a)\beta(b)-\beta(a)\alpha(b)> \rightarrow 1/\sqrt{2}|\alpha\beta-\beta\alpha> \equiv |S> \quad \text{(A7)}$$

$$|\Psi_4> = |\Phi_4> = 1/\sqrt{2}|\psi_1(a)\psi_2(a)-\psi_2(a)\psi_1(a)>|\beta(a)\beta(a)> \rightarrow |\beta\beta> \equiv |T_-> \quad \text{(A8)}$$

where the total wave functions can be replaced by the nuclear spin triplet functions T_+, T_o, T_-, and the singlet function S. Equations A5−A8 are valid in the absence of a magnetic field where the energy difference between the three degenerate triplet states and the singlet state is given by the coupling constant J. Equation A1 is valid for a strong magnetic field where $J \gg |\nu_1-\nu_2|$.

JA962903R